LA-UR-99-2647

Title: **Model Inversion Using Bayesian Inference And Genetic Algorithms Part III: Chemical Potential and Phase Diagram Determination**

Author(s): Brian J. Reardon, MST-6

Submitted to:

Model Inversion Using Bayesian Inference And Genetic Algorithms Part III: Chemical Potential and Phase Diagram Determination

Brian J. Reardon, MST-6, Los Alamos National Laboratory, Los Alamos, NM 87545

Abstract

The determination of phase diagrams from a minimum number of data sets is problematic both from the stand point of being an under determined inverse problem and from that fact that it is also ill-posed. This arises from the fact that the calculated composition is a function of temperature while experimentally, both the composition and temperature are measured observables that contain a significant amount of uncertainty. In an effort to determine the proper values for the liquidus equations, a genetic algorithm was used with Bayesian statistics to assist in the analysis of the final population. The component melting points and the experimentally observed temperatures were treated as parameters to be optimized within their known uncertainty limits. The GA was then able to optimize the heats of fusion of UO_2 and BeO to their experimentally observed values using data collected at temperatures considerably lower than the melting points of the pure components. Furthermore, the distribution of final optimized models were plugged into the forward problem to determine the uncertainty of the phase boundaries.

1.0 Introduction

1.1 Inverse and Ill Posed Problems in Materials Science and Engineering

There is an ever increasing need in materials science and engineering to fit the parameters of models, which are to be used in a predictive capacity, using underdetermined experimental data sets. Model inversion of this type falls under the general category of inverse and ill – posed problems and can often be cast into the framework of Bayesian statistics (Tarantola, 1987). Such problems include determining powder densification models from limited density data, state function determination, and mechanical threshold strength determination from mechanical tests also with a high degree of uncertainty. In all of these examples, model parameters must be optimized using limited and uncertain data sets that leave the inversion underdetermined. Likewise, if the models are to be used in a predictive capacity, there is a need to be able to quantify the expected deviation of the model from reality.

This report shows how a fuzzy logic based multi-objective genetic algorithm (GA) (Reardon 1999) can be used as a Bayesian Inference Engine (BIE) to evolve a posterior probability density (PPD) of the model parameter vector space:

$$M_i = \{m_1, m_2, m_3, \ldots, m_N\}^T \qquad \text{Eq. 1}$$

where M_I is a particular model to be tested, m_J is one of the N parameters used in the model and T signifies the transpose of the vector. The GA evolves a set or population of M_I's which effectively defines the PPD. Once the PPD has been sufficiently determined by the GA, parameter vectors are selected and used in the physics of the forward problem, for future experimental conditions, to evaluate the predictive capacity of the model.

The problem to be addressed through the use of GA's and Bayesian inference lies in the general realm of multiple component phase diagram determination. From nuclear fuels to alloy design, understanding, calculation and measurement of phase

diagrams is the backbone of the structure – property – processing relationship. Unfortunately, as the materials science community moves towards multi-component systems (phase diagrams containing 4 or more components) computation becomes considerably more complex and with this complexity comes an increased concern for both the accuracy of the models and the effects of experimental error propagation. There is currently no quantitative way of addressing this issue, and thus, the main challenge faced by the materials science community is estimating the boundaries of multiple component phase diagrams given sparse and uncertain experimental data. This report will show that a multiobjective genetic algorithm (GA) coupled with Bayesian statistics can more accurately link the limited and uncertain experimental thermodynamic data to the phase diagram model of interest.

Published experimental thermodynamic information is not absolutely precise but altered by errors estimated by the author. These errors are intrinsic to both the method and to the devices used to do measurements. Consequently, different sources of information may provide values laying in a broad domain for the same thermodynamic function. A related issue is that the thermodynamic data required for the phase diagram calculation do not usually form a consistent set of data. The Gibbs' free energy retrieved by integration from the heat capacity dependency with respect to the temperature may differ from the values that are retrieved from emf experiments or calculated from the partial pressure of the gaseous phases in the system.

There are a number of other concerns with the experimental verification and determination of phase diagrams. First, high temperature experiments are inherently more uncertain in both temperature and composition. Additionally, the cost and hazards of working with materials at high temperature are greater. Lastly, the formation of metastable states often occurs causing two problems. First, the formation of metastable states experimentally results in an inaccurate equilibrium phase diagram. Second, there exists the possibility of unknowingly forming metastable states not predicted under proper equilibrium conditions. In either case there is a substantial need to calculate a phase diagram along with providing at least a qualitative measure of its reliability and

metastability. In addition to determining the equilibrium and metastable states, such calculations can be used as a guide in experimental design to reduce the number of experiments and to extract as much information as possible from experiments already conducted.

As an example of the GA's ability to be used in the calculation of phase diagrams, consider the simple eutectic diagram of the binary system, UO_2-BeO (Budnikov *et al*. (1958) and Bergeron and Risbud (1984)). The liquid phase of this system closely approximates an ideal solution and thus the Gibbs free energy of the liquid can be stated as:

$$\Delta G_l = RT\left(x \ln x + (1-x) \ln (1-x)\right) \qquad \text{Eq. 2}$$

where R is the gas constant, T is the absolute temperature, and x is the mole percent of BeO. Likewise, it is assumed that solid UO_2 and BeO are completely insoluble. Therefore, the free energy of each component at any temperature is a function of the difference of the free energies between the solid and liquid phases. Therefore:

$$\Delta G^{UO_2} = G_s^{UO_2} - G_l^{UO_2} = -\Delta H_f \ln \frac{T_M^{UO_2}}{T} \qquad \text{Eq. 3}$$

and

$$\Delta G^{BeO} = G_s^{BeO} - G_l^{BeO} = -\Delta H_f \ln \frac{T_M^{BeO}}{T} \qquad \text{Eq. 4}$$

With the free energies in hand, the compositions of the liquidus boundary can be found by using the taunt string method. In other words, by finding the tangent of Eq. 1 to each free energy point at x = 0and 1 as defined in Eqs. 3 and 4:

$$\frac{\Delta G_l\left(x_{UO_2}\right) - \Delta G^{UO_2}}{x_{UO_2} - 0} = \frac{\partial \Delta G_l\left(x_{UO_2}\right)}{\partial x_{UO_2}} \qquad \text{Eq. 5}$$

and

$$\frac{\Delta G^{BeO} - \Delta G_l\left(x_{BeO}\right)}{1 - x_{BeO}} = \frac{\partial \Delta G_l\left(x_{BeO}\right)}{\partial x_{BeO}} \qquad \text{Eq. 6}$$

Solving for X_{UO2} and X_{BeO}:

$$x_{UO_2} = 1. - \exp\left[\frac{-\Delta H_{UO_2}}{RT_{UO_2}} \log\left(\frac{T_M^{UO_2}}{T_{UO_2}}\right)\right] \qquad \text{Eq. 7}$$

and

$$x_{BeO} = \exp\left[\frac{-\Delta H_{BeO}}{RT_{BeO}} \log\left(\frac{T_M^{BeO}}{T_{BeO}}\right)\right] \qquad \text{Eq. 8}$$

Equations 7 and 8 then become the objective functions used in the optimization where the goal is to find the values of ΔH_{UO2}, ΔH_{BeO}, T_M^{UO2}, and T_M^{BeO} given experimentally observed values for X_{BeO} at T_{BeO} and X_{UO2}at T_{UO2}. While ΔH_{UO2}, ΔH_{BeO}, T_M^{UO2}, and T_M^{BeO} are experimentally accessible, the temperatures at which the experiments must be conducted result in a significant amount of uncertainty in their actual values. Consequently, the goal in this work is to determine the values for ΔH_{UO2}, ΔH_{BeO}, T_M^{UO2}, and T_M^{BeO} given the low temperature data points of the eutectic phase diagram. The main problem with this approach is that even if a large number of data points were available, the problem would still be underdetermined since x is a function of T and they both have associated uncertainties. Thus, to facilitate the optimization, T_{BeO} and T_{UO2} will also be treated as parameters to be optimized in which their respective search ranges are the errors associated with their experimental uncertainty. Consequently, the optimization problem at hand is multi-objective since numerous data points on the liquidus can be available and the problem is also multi-variate since the model parameter vector has the form:

$$M=\{\Delta H_{UO2}, \Delta H_{BeO}, T_M^{UO2}, T_M^{BeO}, T_{UO2}\ldots, T_{BeO}\ldots, r\}^T \qquad \text{Eq. 9}$$

Where T_{UO2}… refers to the fact that there may be many UO_2 liquidus data points and T_{BeO}… refers to the same. The parameter, r, is a dummy variable incorporated into the optimization to confirm that the GA is performing correctly and not succumbing to genetic drift.

In this work the experimentally derived data points will be the eutectic composition. Thus, there are two data points: $X_{UO2} = X_{BeO} = 0.68 \pm 0.05$ and the parameter search ranges are: $10000 \text{ cal/mol} \le \Delta H_{UO2} \le 30000 \text{ cal/mol}$, $10000 \text{ cal/mol} \le \Delta H_{BeO} \le 30000 \text{ cal/mol}$, $3000K \le T_M^{UO2} \le 3200K$, $2700K \le T_M^{BeO} \le 2900K$, $2423K \le T_{UO2}, T_{BeO} \le 2463K$, and $0.0 \le r \le 1.0$. The temperature search ranges are obtained from what is considered to be the uncertainty in the measured values. The heat of formation search ranges were intentionally made very broad to emulate the fact that for any arbitrary system the heats of formation may not be known.

1.2 Bayesian Statistics in Model Inversion

Consider a model parameter vector such as the one defined in Eq. 9 and also consider a data vector defined as:

$$D=\{X_{UO2}\ldots, X_{BeO}\ldots\}^T. \qquad \text{Eq. 10}$$

The goal of Bayesian analysis is to come up with a way of accepting or rejecting a particular model (M) or hypothesis given an experimental data set (D) and prior knowledge about the problem. Thus, in Bayesian statistics, the model or hypothesis is assigned a probability of acceptance and the total probability distribution function (PDF) of a series of models being tested makes up what is commonly called the posterior probability density (PPD). This goal is achievable through the central tenant of Bayesian statistics, Bayes' Theorem:

$$\sigma(M \mid D) = \frac{P(M,D)}{P(D)} = \frac{P(D \mid M)P(M)}{\int P(D,M)dM} \qquad \text{Eq. 11}$$

which is essentially the definition of conditional probability. This rule was first proposed by Rev. Thomas Bayes and published posthumously in 1763 but has been fairly ignored up until the last 20 years due to the computational difficulties in evaluating the probability integrals (Bayes, 1763). This theorem says that the conditional probability of a model being correct given a set of data is a ratio of the PDF of M and D to the PDF of D alone. The term P(D | M) is not a PDF but a likelihood function. Thus, while the individual components of P(D | M) are probabilities, the function itself does not integrate to 1.0.

Bayes' rule as written above differs considerably from classical frequentist statistics because of the dependence of the PPD on the prior PDF, P(M). P(M) often contains subjective information about the problem that the experimentalist has *a priori*. Another major departure from frequentist statistics is the way the PPD is updated as new experimental data becomes available. The frequentist view point is that P(D) should be considered an unchanging distribution and that it is inappropriate to try to assign a probability of correctness to a hypothesis.

Consequently, Bayes' Rule provides the scientist with a tool that classical statistics is not capable or providing, namely, a mathematical formalization of the scientific method. When a phenomenon is observed, a hypothesis explaining the event is created often with the observer's own bias and experience in mind. This hypothesis is then tested against new experimental data and if the data supports the hypothesis then the belief in or probability of acceptance of the hypothesis increases. An excellent introduction to the Bayesian approach to hypothesis testing can be found in Chapter 4 of Antelman (1997).

The main difficulty in using Bayes' rule, lays in the evaluation of the denominator:

$$P(D) = \int P(D,M)dM, \qquad \text{Eq. 15}$$

where the integral is formally carried over the entire N-dimensional model parameter space. The accurate and fast approximation of the integration of these N-dimensional,

discontinuous PDF's is the topic of many papers. Duijndam (1988a, 1988b) discussed the used of Bayes' Rule in model inversion and accomplished the above integration by assuming the PPD had a Gaussian shape then optimized the Gaussian parameters using least squares. Unfortunately, most PPD's are not Gaussian in nature and thus other techniques were needed. These techniques include Monte Carlo integration, Gibb's Sampling, and genetic algorithms (Sen and Stoffa ,1992, 1996; Sen et al., 1993; Mallick, 1995; Gerstoft, 1998).

The PPD is itself a difficult function to visualize due to its multidimensionality and its change with every new experimental data point. However, once the PPD is derived, regardless of the method, a number of important parameters describing it can be easily calculated.

The mean model can be calculated using the following formula which is a standard definition in most statistics books:

$$\langle M \rangle = \int M \sigma(M \mid D) dM \qquad \text{Eq. 16}$$

Likewise, the *a posteriori* model covariance matrix is given by:

$$C_M = \int (M - \langle M \rangle)(M - \langle M \rangle)^T \sigma(M \mid D) dM. \qquad \text{Eq. 18}$$

The covariance matrix provides a number of useful parameters. The standard deviation associated with the mean model is obtained through the square roots of the diagonal elements of C_M. Normalization of C_M through:

$$C_{ij} = \frac{C_{ij}}{\sqrt{C_{ii}}\sqrt{C_{jj}}} \qquad \text{Eq. 20}$$

produces the correlation matrix.

With C_M determined, a principle component analysis (PCA) will provide valuable insight on how well the GA is converging and what model parameters are most significant or sensitive. In PCA the data of the C_M is transformed into a new set of axes of the same number which are orthogonal to each other and are ordered based on the variance associated with that axis. The principle components of C_M can be obtain by computing its set of eigenvalues (Λ) and corresponding orthogonal eigenvectors (U) such that:

$$C_M = U\Lambda U^T \qquad \text{Eq. 21}$$

is satisfied. In a d-dimensional variable space there are d eigenvalues or principle components. However, many principle components may have small variances and thus the intrinsic dimensionality of C_M is k where $k<d$.

In the context of a PPD evolved by a GA, PCA is a powerful tool that assists in overcoming many deficiencies in GA's. First, as the GA evolves the population, the eigenvalues of C_M asymptotically approach limits. When the rate of convergence reaches an acceptable minimum the GA can be stopped. Second, the largest eigenvalues and their corresponding eigenvectors indicate the most significant variables or groups of variables in the model given the available data. Thus, PCA provides a sensitivity analysis for the variables in the model.

Once a PPD has been determined to be reliable based on the stabilization of the eigenvalues, an optimum model can be selected.

1.3 Genetic Algorithms in Model Inversion and Parameter Optimization

A detailed account of how a GA operates has been provided elsewhere (Reardon 1998a, 1998b, 1999). In short, a GA randomly generates a set or population of parameter vectors M_i's where i = 1 to N and N is the population size. This initial selection, which occurs within parameter ranges set by the user, constitutes the *a priori* information used in Bayes' Theorem. From this set, parameter vectors that satisfactorily solve the optimization problem are selected. The selected members, which are each

defined by a haploid binary string, exchange string components and thus create new members. The bits of the new member's strings are then randomly flipped with a small degree of probability from 1 to 0 or vice versa. The final members are then inserted into the next generation. Once the next generation is filled the GA starts over with selection, crossover and mutation.

Since the GA acts as a BIE in that it uses Bayes' Theorem to select members in the population for crossover, the output of the GA is the PPD. The generation of a PPD now allows for many of the statistical tools available in Bayesian statistics to be used in the analysis of the output of the GA. Namely from the PPD we can derive <M> and C_M. The beauty of this approach is that the PPD can be generated at virtually no extra cost. Following the method outlined by Sen and Stoffa (1992), a 2-D array of M X B is reserved where M is the number of parameters and B is the number of values each variable can take (i.e. the number of bins). For each model at each generation an unnormalized PPD, $\sigma(M)$, is computed and stored in the proper position in the bin array for each model parameter comprising each model. At the end of the GA run the model parameter PPD values are normalized. Also in a vector of length M, each component of M $\sigma(M)$ is stored and summed with the correspond values from the other models. This vector provides <M>. C_M is determined by summing up $MM^T \sigma(M)$ in a square array of MM for each model and at the end of the run subtracting $<M><M>^T$. The FORTRAN 90 code used to evaluate these quantities was presented previously (Reardon 1999).

Once the PPD, <M>, and C_M have been sufficiently determined, the GA can be stopped and optimal model parameter vectors can be selected and used in the physics of the forward problem for conditions that have not been experimentally tested.

2.0 The UO_2-BeO Liquidus

Figures 1-4 show the evolution of the eigenvalues as a function of generation. The smallest eigenvalue and thus least significant is shown in figure 1. Examination of the first eigenvector in Table I corresponding to the first eigenvalue indicates that this eigenvector is dominated by the dummy variable incorporated into the optimization to ensure the proper performance of the GA. If the GA is performing correctly, then the

dummy variable should remain random with respect to generation number whereas if the GA is succumbing to genetic drift, then the random variable will converge to some value within its search range. Additionally, since the dummy variable is not used in the objective functions, its sensitivity should be very low. If a variable were found to have a sensitivity lower than the dummy variable, then one could conclude that the value of that variable has no impact on the model performance whatsoever.

Figure 2 shows two eigenvalues that are approximately two orders of magnitude larger than that of figure 1. These two eigenvalues have eigenvectors dominated by the melting point and eutectic temperature variables. The next two largest eigenvalues have eigenvectors also dominated by the melting point and eutectic temperature variables. The final two eigenvalues are approximately 4 orders of magnitude larger than the smallest eigenvalue and are thus the most significant. These eigenvalues have eigenvectors dominated by the two heats of fusion and thus one can conclude that for this optimization, the heats of fusion are the most important variables. Of course, the importance of the melting points and the final eutectic temperature should not be discounted. In this optimization, the search ranges for the temperature variable were set to the known experimental uncertainties and, thus one would not expect any real convergence or sensitivity of these variables within such confined search ranges.

Figures 5-8 show the expectation values for the optimized parameters as a function of generation. Figure 5 shows the expectation values for the heats of fusion of UO_2 and BeO. ΔH_{UO2} is converging to a value of 23048 cal/mol whereas ΔH_{BeO} is converging to a value of 16596 cal/mol. The accepted values for the heat of fusion according to Bergeron and Risbud (1984) are ΔH_{BeO} =17000 cal/mol and ΔH_{UO2} = 22900 cal/mol. Thus the GA has done an adequate job at optimizing the most significant parameters in this problem given only two low temperature data points. The expectation values of the melting points (figure 6), eutectic temperatures (figure 7), and the dummy variable (figure 8) do not indicate that the population as a whole is converging to a specific value. This conclusion is derived from the fact that the average value for generation 0 and generation 100 do not differ significantly. However,

examination of the standard deviations of the population are necessary to confirm or deny this assumption.

Figures 9-12 show the standard deviation of the expectation value as a function of generation for all of the variables. Again, the heats of fusion are clearly converging as is evidenced by the standard deviation that has dropped to approximately 10% of the expectation value. The standard deviation for the melting points (figure 10), eutectic temperatures (figure 11), and the dummy variables (figure 12) do not show any sign of convergence. Again, this would be expected since these parameters were not deemed significant in the PCA and since the search range of each variable was set well within the known experimental uncertainty.

The final figure, figure 13, shows the UO_2-BeO eutectic phase diagram calculated using the evolved PPD. The scatter shown in the phase boundaries is well within the know uncertainty of the current phase diagram. The main difference, of course, was that this diagram was determined with only two low temperature data points.

3.0 Conclusions

The determination of phase diagrams from a minimum number of data sets is problematic both from the standpoint of being an under determined inverse problem and from that fact that it is also ill-posed. This arises from the fact that the calculated composition is a function of temperature and both the composition and temperature are measured observables that contain a significant amount of uncertainty. In an effort determine the proper values that go into the liquidus equations, a genetic algorithm was used with Bayesian statistics to assist in the analysis of the final population. By treating the melting points and the experimentally observed temperatures as parameters to be optimized within their known uncertainty limits, the GA was able to optimize the heats of fusion of UO_2 and BeO to their experimentally observed values using data collected at considerably lower temperatures. Furthermore, the distribution of final optimized models were plugged into the forward problem to determine the uncertainty of the phase boundaries.

4.0 Acknowledgments

Funded by the Department of Defense, the Department of Energy and Los Alamos National Laboratory which is operated by the University of California under contract number W-7405-ENG-36.

5.0 References

G. Antelman, 1997, “Elementary Bayesian Statistics,” Eds. A. Madansky, R. McCulloch, Edward Elgar Publishing, Inc., Lyme, NH.

T. Bayes, 1763, “An Essay towards solving a problem in the doctrine of Chances,” Philosophical Transactions of the Royal Society, 53, 370-418.

C. G. Bergeron, S. H. Risbud, 1984, “Introduction to Phase Equilibria in Ceramics,” The American Ceramics Society.

P. P. Budnikov, S. G. Tresvyatsky, and V. I. Kushakovsky, 1958, “Binary Phase Diagrams for UO_2-Al_2O_3, UO_2-BeO, and UO_2-MgO,” Proc. U.N. Intern. Conf. Peaceful Uses At. Energy, 2nd, Geneva, 6, 127.

A. J. W. Duijndam, 1988a, “Bayesian Estimation in Seismic Inversion. Part I: Principles,” Geophysical Prospecting, 36, 878-898.

A. J. W. Duijndam, 1988b, “Bayesian Estimation in Seismic Inversion. Part II: Uncertainty Analysis,” Geophysical Prospecting, 36, 899-918.

P. Gerstoft and C. F. Mecklenbräuker, 1998, “Ocean Acoustic Inversion with Estimation of *a posteriori* probability distributions,” Journal of the Acoustical Society of America, 104, 2, 808-819.

S. Mallick, 1995, “Model-based Inversion of Amplitude-variations-with-offset Data Using a Genetic Algorithm,” Geophysics, 60, 4, 939-954.

B. J. Reardon, 1998a, “Fuzzy Logic Vs. Niched Pareto Multiobjective Genetic Algorithm Optimization,” Modeling and Simulation in Materials Science and Engineering, 6, 717-734, 1998, http://www.iop.org/Journals/ms

B. J. Reardon, 1998b, “Optimization of Densification Modeling Parameters of Beryllium Powder Using a Fuzzy Logic Based Multiobjective Genetic Algorithm,” Modeling and Simulation in Materials Science and Engineering, 6, 735-746, http://www.iop.org/Journals/ms

B. J. Reardon, 1999, “Model Inversion Using Bayesian Inference and Genetic Algorithms,” LA-UR-99-1980, Los Alamos National Laboratory, Los Alamos, NM 87545, April, http://lib-www.lanl.gov//la-pubs/00326698.pdf.

M. K. Sen, B. B. Bhattacharya, P. L. Stoffa, 1993, “Nonlinear inversion of resistively sounding data,” Geophysics, 58, 4, 496-507.

M. K. Sen and P. L. Stoffa, 1992, “Rapid sampling of model space using genetic algorithms: Examples from seismic waveform inversion,” Geophysics Journal International, 108, 281-292.

M. K. Sen and P. L. Stoffa, 1996, “Bayesian inference, Gibb’s sampler and uncertainty estimation in geophysical inversion,” Geophysical Prospecting, 44, 313-350.

A. Tarantola, 1987, “Inverse Problem Theory, Methods for Data Fitting and Parameter Estimation,” Elsevier, Amsterdam.

6.0 Tables

Table I. The final eigenvectors.

Parameter	λ_1	λ_2	λ_3	λ_4	λ_5	λ_6	λ_7
ΔH_{UO2}	1.0775e-06	0.0013589	-0.00031904	-0.00074791	-0.0029665	0.95527	0.29572
ΔH_{BeO}	-5.8269e-07	0.0010914	-0.00024326	-0.0026017	-0.00079303	0.29572	-0.95527
T_M^{UO2}	0.00024235	0.17291	-0.024217	0.00031154	-0.98463	-0.0033100	-4.3217e-06
T_M^{BeO}	-0.00020423	0.33294	-0.12370	-0.93279	0.061220	-0.0017825	0.0023496
T_{UO2}	-0.00035270	-0.57099	-0.81067	-0.10158	-0.080366	0.00022275	-3.3683e-05
T_{BeO}	0.00050685	0.73022	-0.57177	0.34580	0.14241	-0.00044885	-0.00021896
r	-1.0000	0.00054542	1.5508e-05	0.00040168	-0.00015071	1.3600e-07	2.7289e-07

7.0 Figures

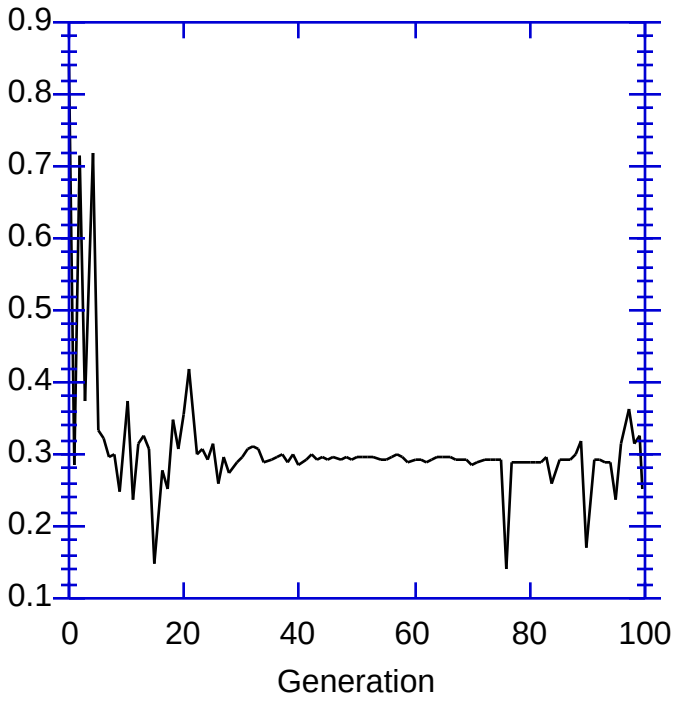

Figure 1. The smallest eigenvalue, λ_1, as a function of generation.

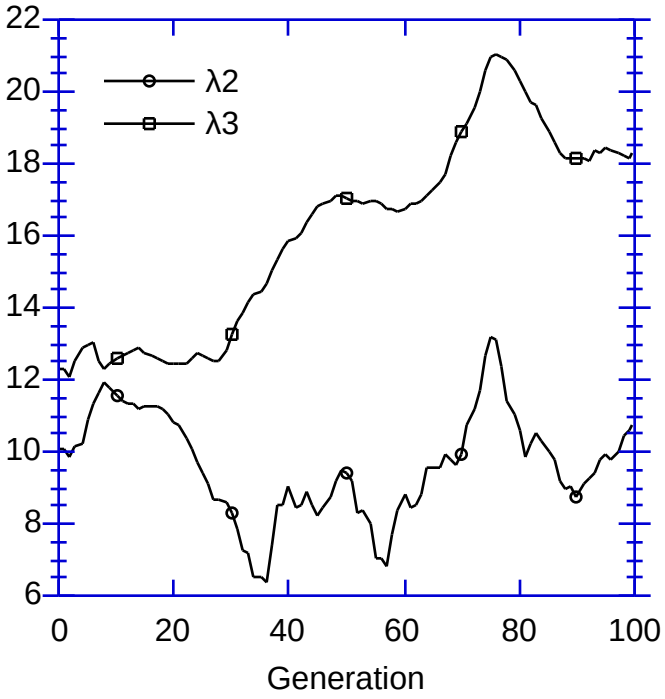

Figure 2. λ_2 and λ_3 as a function of generation.

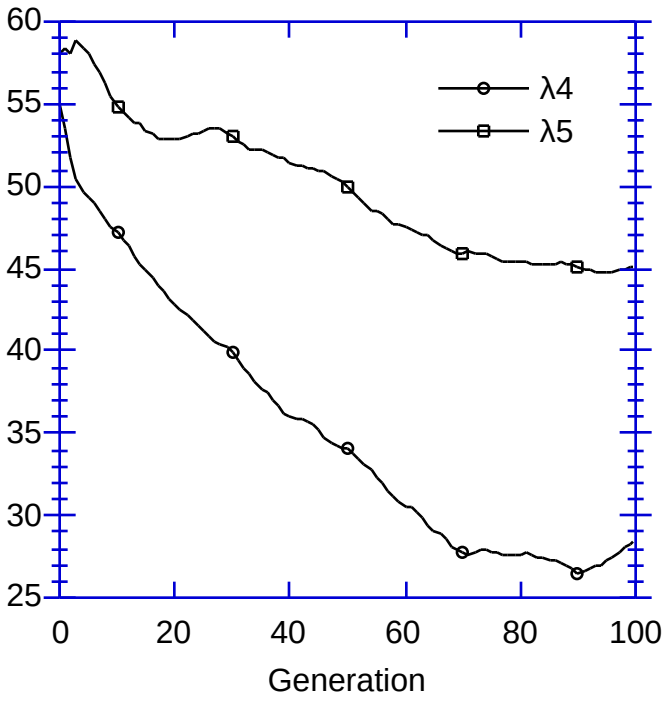

Figure 3. λ_4 and λ_5 as a function of generation.

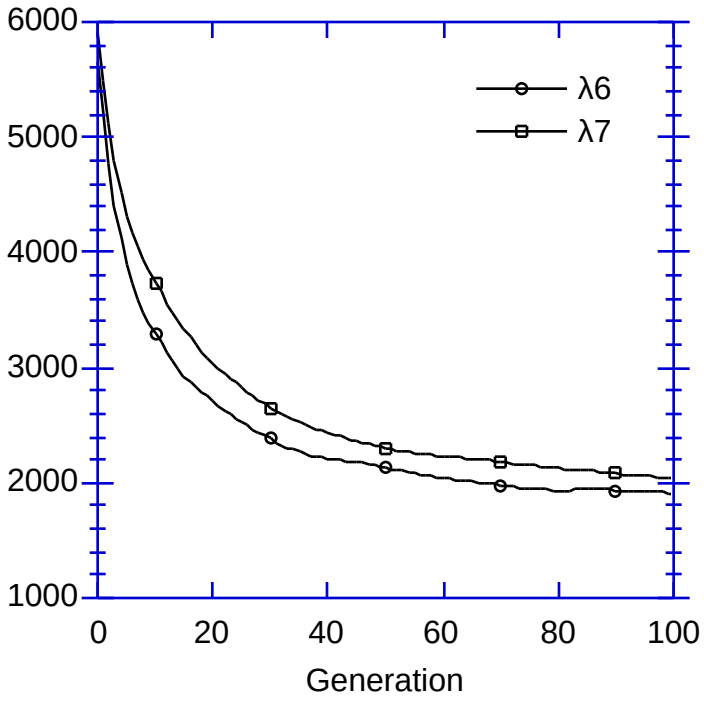

Figure 4. The two largest eigenvalues, λ_6 and λ_7, as a function of generation.

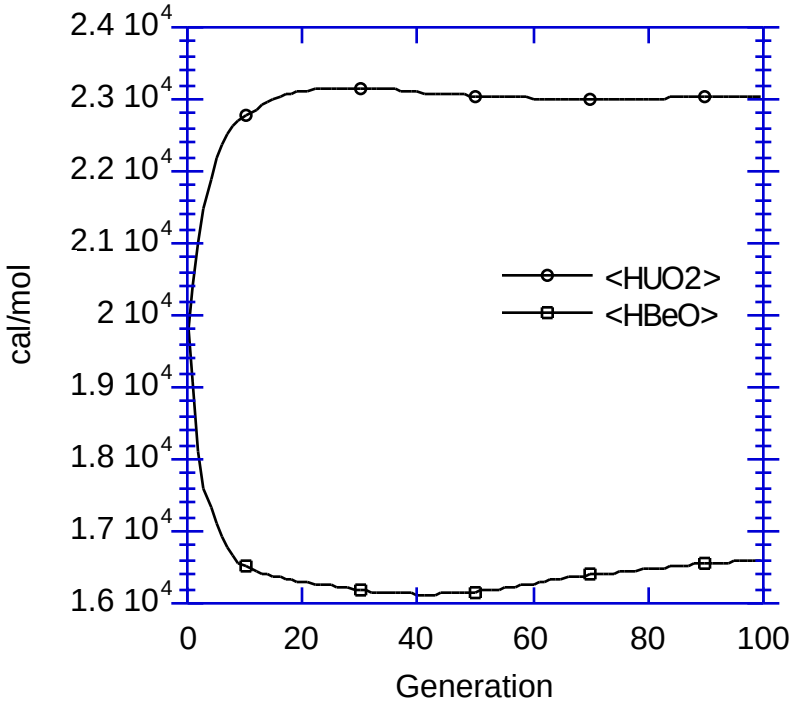

Figure 5. $< \Delta H_{UO2} >$ and $< \Delta H_{BeO} >$ as a function of generation.

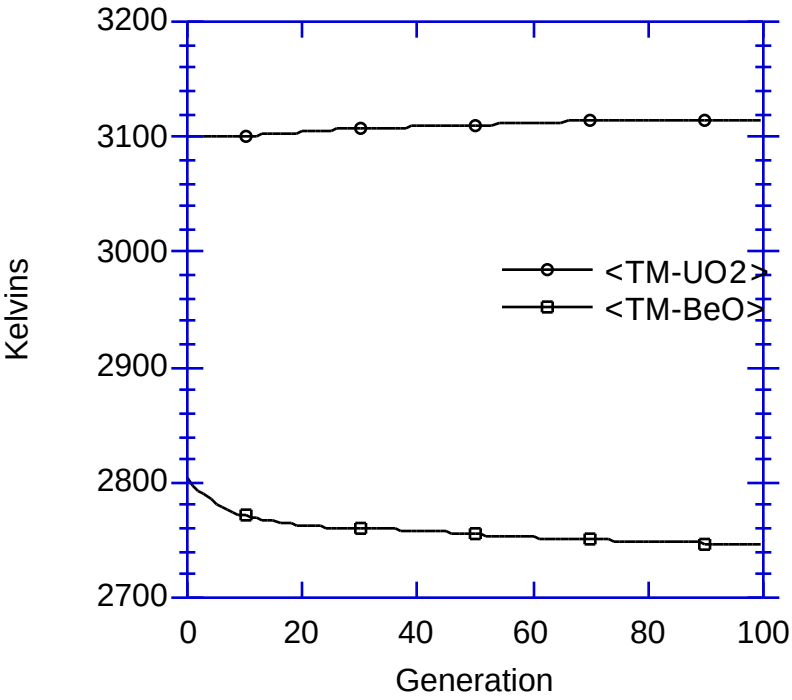

Figure 6. $<T_M^{UO2}>$ and $<T_M^{BeO}>$ as a function of generation.

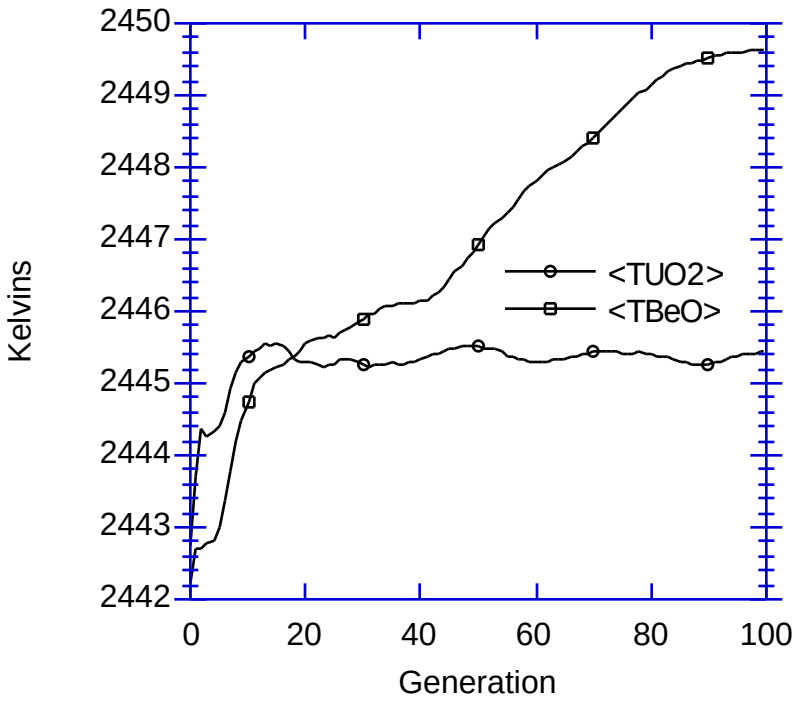

Figure 7. $<T_{UO2}>$ and $<T_{BeO}>$ as a function of generation.

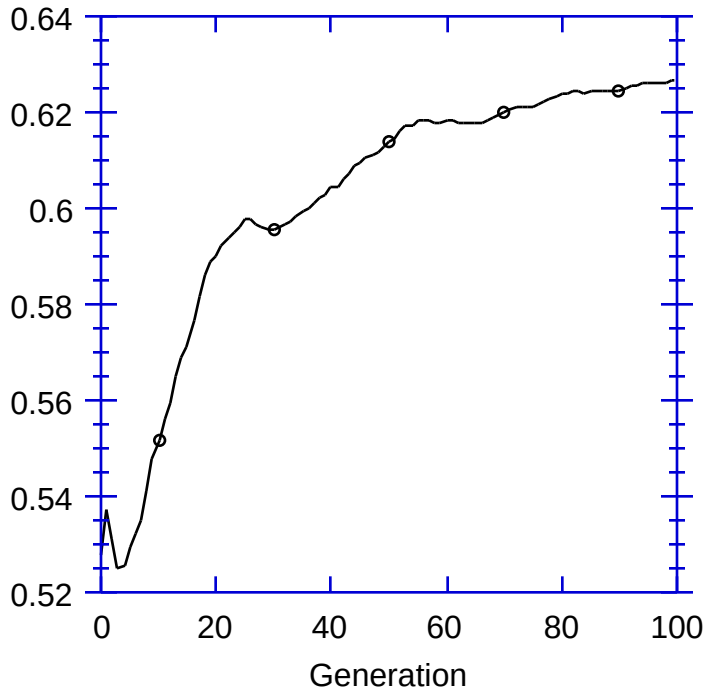

Figure 8. <r> as a function of generation.

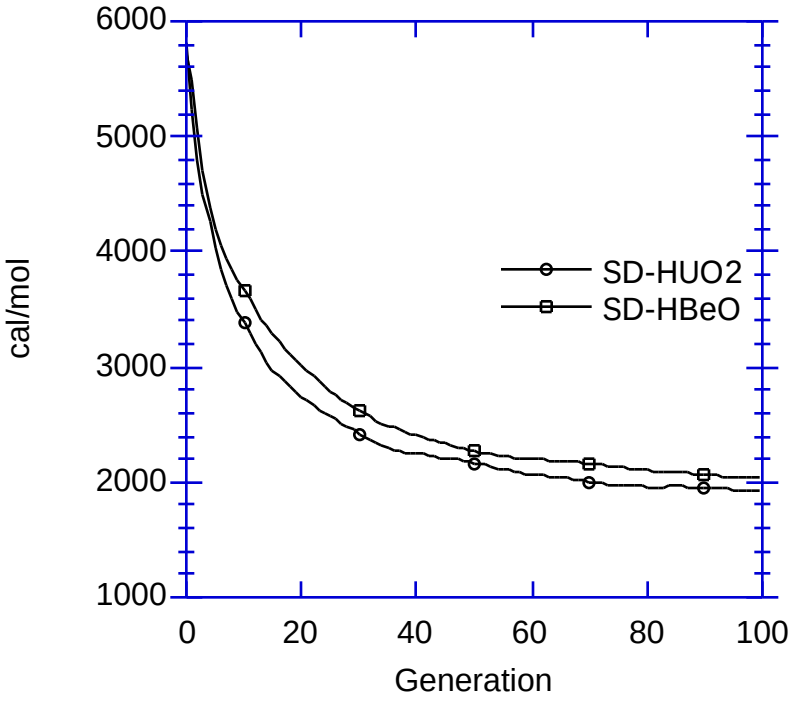

Figure 9. The standard deviation of ΔH_{UO2} and ΔH_{BeO} as a function of generation.

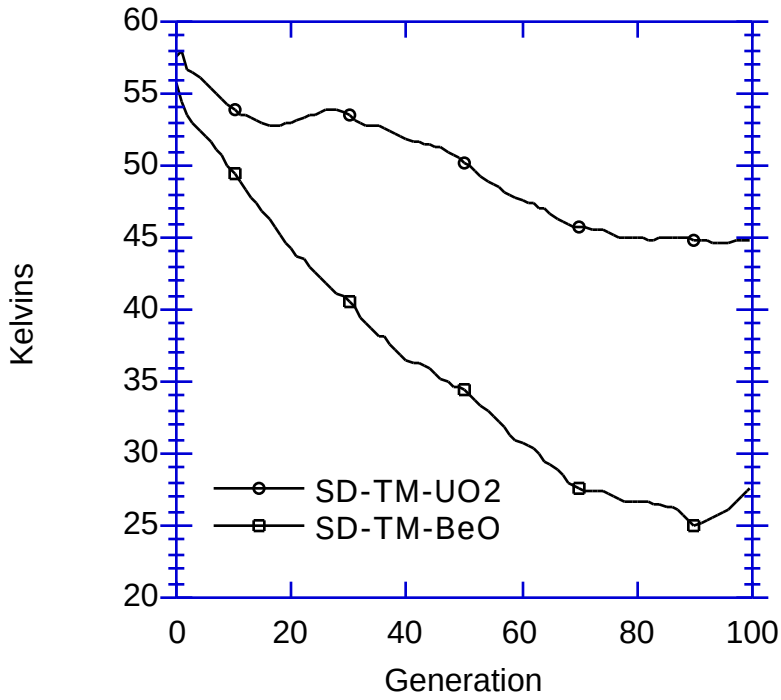

Figure 10. The standard deviation of T_M^{UO2} and T_M^{BeO} as a function of generation.

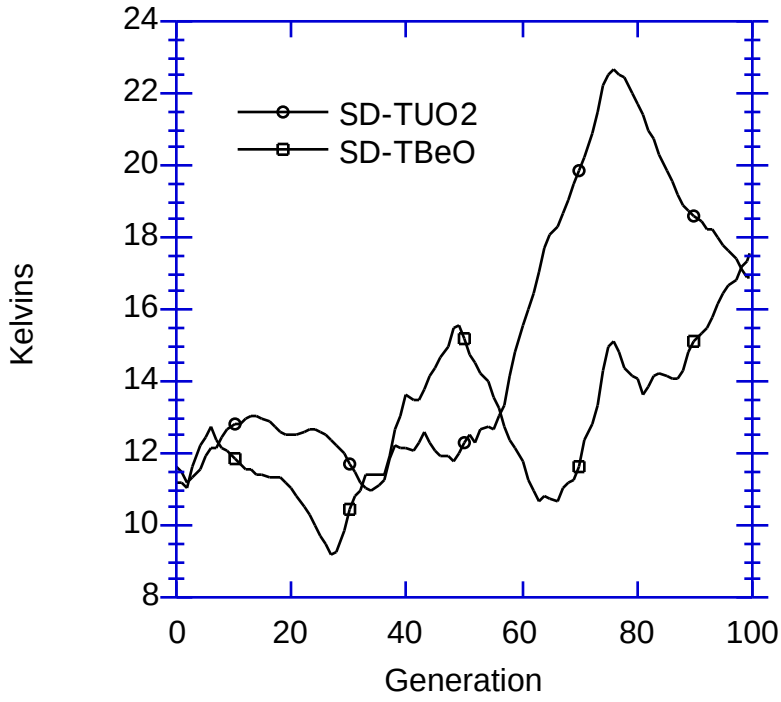

Figure 11. The standard deviation of T_{UO2} and T_{BeO} as a function of generation.

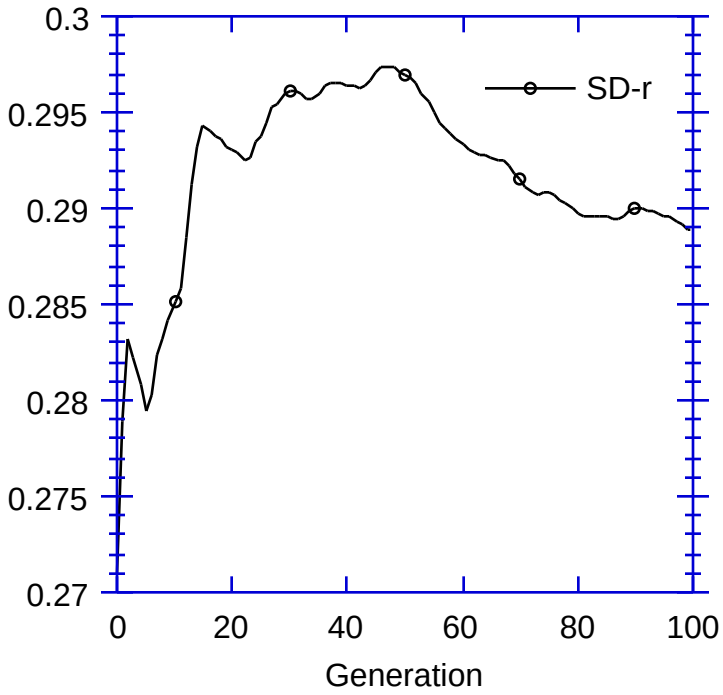

Figure 12. The standard deviation of r as a function of generation.

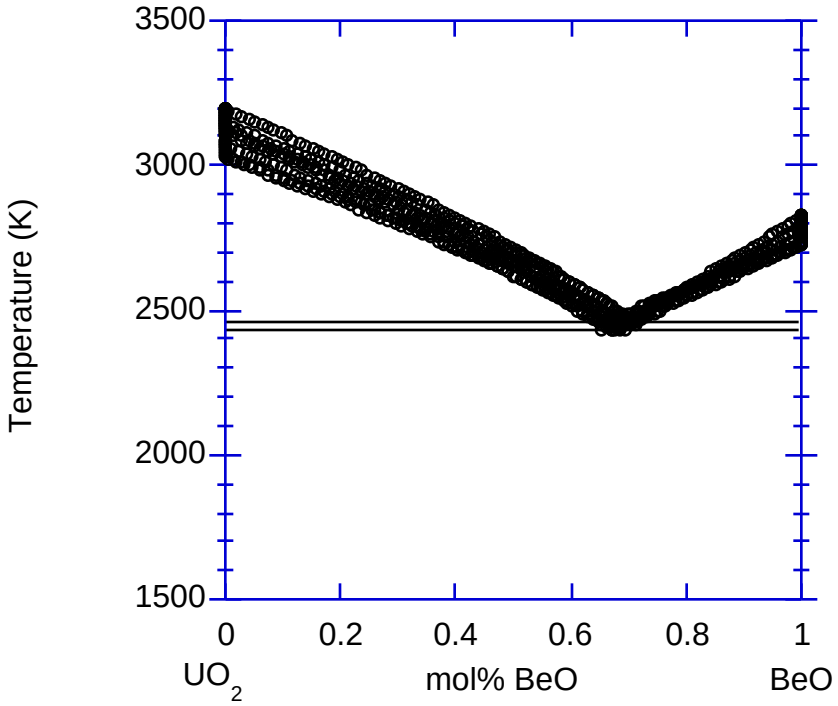

Figure 13. The calculated UO_2-BeO phase diagram determined from the evolved PPD.